Received: 22 November 2021 | Revised: 15 April 2022 | Accepted: 26 April 2022

DOI: 10.1002/joc.7681

RESEARCH ARTICLE

International Journal of Climatology RMetS

The Orinoco low-level jet during El Niño–Southern Oscillation

Alejandro Builes-Jaramillo | **Johanna Yepes** | **Hernán D. Salas**

Facultad de Arquitectura e Ingeniería, Institución Universitaria Colegio Mayor de Antioquia, Medellín, Colombia

Correspondence
Alejandro Builes-Jaramillo, Facultad de Arquitectura e Ingeniería, Institución Universitaria Colegio Mayor de Antioquia, Carrera 78 # 65-46 Bloque Patrimonial piso 2, 050034 Medellín, Colombia.
Email: luis.builes@colmayor.edu.co

Funding information
Institución Universitaria Colegio Mayor de Antioquia

Abstract

This study shows the influence of El Niño–Southern Oscillation (ENSO) over the seasonal and diurnal variability of the Orinoco low-level jet (OLLJ) during the December–January–February (DJF) season. Results show changes in the occurrence and intensity of the OLLJ winds during the phases of ENSO (El Niño and La Niña) in relation to Neutral conditions. During El Niño (La Niña), the OLLJ days decrease (increase) over the mid and exit of the OLLJ corridor. Furthermore, the mean wind vertical profiles (and the intensity of the diurnal cycle) decrease (increase) with values ranging from 5 to 9 m·s^{-1}. We highlight that the OLLJ days decrease (increase) in January (February) during El Niño (La Niña) up to 24% (15%). These changes are modulated by the pressure gradient between the Atlantic subtropical high and the near-equatorial trough regions that decreases (increases) during El Niño (La Niña) and thus induces a decrease (increase) of the OLLJ winds. Moreover, the water vapour flux and precipitation reduce during both phases of ENSO along the OLLJ corridor. This work shows new insights on the OLLJ features during ENSO, which contributes to improving our understanding of the processes that influence the hydro-climatology of northern South America.

KEYWORDS

ENSO, moisture transport, near-equatorial trough, North Atlantic subtropical high, Orinoco low-level jet, tropical rainfall

1 | INTRODUCTION

The Orinoco low-level jet (OLLJ) is a climatic feature that is located over the shared plains of Colombia and Venezuela in northern South America. Despite its importance in the hydroclimate of the northeastern South America (Labar *et al*., 2005), it has been understudied or defined as the northern branch of the South American low-level jet (Jones, 2019). At seasonal scales, Montoya *et al*. (2001) and Rueda (2014) have shown that the jet is a predominant boreal winter feature with a core between 1,000 and 850 hPa and mean wind speed around 6–8 m·s^{-1}. Recently, Builes-Jaramillo *et al*. (2022) and Algarra *et al*. (2019) showed that the OLLJ is one of the mechanisms involved in the moisture transport from the tropical North Atlantic (TNA) towards the Amazon River basin and southern South America during December–February (DJF). In contrast, during July–August (JJA) coinciding with the weakest winds along the OLLJ corridor, the cross-equatorial flow (CEF) transports moisture from the Amazon to northern South America (Wang and Fu, 2007). The moisture flux through the jet corridor is associated with the annual cycle of the OLLJ and also with the annual cycle of precipitation over the Orinoco region: strong OLLJ winds coincide with the dry season (DJF) whereas weak jet winds occur during the wet season (JJA) (Builes-Jaramillo *et al*., 2022).

At the regional scale, the origin of the OLLJ has been explained by the pressure gradient between the North Atlantic subtropical high (NASH) and the near-equatorial trough (NET), resulting in the strengthening of the northeasterlies while it is forced by the Coastal Cordillera (northern Venezuela) and the Guianese Shield (Vernekar *et al.*, 2003; Labar *et al.*, 2005; Rueda, 2014). Further south, the OLLJ plays a key role in the transport of pollutants during DJF along the corridor towards Ecuador, increasing the particulate concentrations in northern South America (Rodríguez-Gómez *et al.*, 2021).

At the local scale, Jiménez-Sánchez *et al.* (2020) states that the characteristics of the OLLJ can be explained by four physical mechanisms: a sea breeze penetration, katabatic flow, three expansion fans, and diurnal variation of turbulent diffusivity. These processes act together during the night and maintain the acceleration of the winds in the OLLJ's corridor. The OLLJ, along with the Caribbean LLJ (CLLJ), the Choco LLJ (ChocoJet), the Panamá gap flow, the Guianas LLJ, and the South American LLJ (SALLJ) are part of the seasonal climate features that configures northern south America hydroclimate (Amador, 2008; Gimeno *et al.*, 2016; Espinoza *et al.*, 2020).

At the interannual time scales, anomalous sea-surface temperatures (SSTs) in the tropical Pacific and in the TNA during El Niño–Southern Oscillation (ENSO) are considered the main climatic drivers of the northern South America hydroclimate (Enfield and Mayer, 1997; Enfield *et al.*, 1999; Poveda *et al.*, 2011; Viegas *et al.*, 2019; Durán-Quesada *et al.*, 2020). Previous studies suggest that ENSO modulates CLLJ and ChocoJet in different ways. For instance, Amador *et al.* (2016) states the CLLJ is strong (weak) during El Niño (La Niña) in the boreal summer, whereas it is weak (strong) during El Niño (La Niña) in the boreal winter. In contrast, the ChocoJet winds are stronger during La Niña and weaker during El Niño phases in the boreal Autumn (Poveda and Mesa, 2000; Yepes *et al.*, 2019). According to Serna *et al.* (2018), both El Niño canonical and El Niño Modoki diminish the wind speeds of the CLLJ and Chocojet during the first trimester; however, during the last two trimesters of the year CLLJ winds are stronger and Chocojet winds are weaker with respect to Neutral conditions for both El Niño phases. At submonthly timescales, García-Martínez and Bollasina (2020) suggest that ENSO and MJO modulate the intensification and prolong the CLLJ life cycle. Whereas SALLJ is stronger and more frequent during El Niño events over the central Andes of Bolivia and Paraguay (Montini *et al.*, 2019), the northern branch of the SALLJ (Montoya *et al.*, 2001; Labar *et al.*, 2005; Torrealba and Amador, 2010; Rueda, 2014; Jiménez-Sánchez *et al.*, 2019; Jiménez-Sánchez *et al.*, 2020) does not exhibit phasing with ENSO episodes according to Jones (2019).

The characteristics of the OLLJ at the interannual and other long-term timescales are of utmost importance. For instance, OLLJ might play a significant role in the long dry seasons over the Amazon, via the reduced moisture transport from oceanic sources to the Caribbean and the northern South America (Agudelo *et al.*, 2019). Also, it would change as the cross-equatorial flow strengthens (weakens) during boreal winter (summer) under deforestation scenarios in the Amazon basin (Ruiz-Vásquez *et al.*, 2020). Furthermore, Salas *et al.* (2020) studied nonlinear relationships between the OLLJ and precipitation interannual anomalies during ENSO, suggesting an important link between the OLLJ moisture transport and precipitation anomalies over the northernmost part of the Amazon river basin (southern Colombia). Hence, understanding the mechanisms that modulate the OLLJ is important to advance in the diagnosis and modelling of the regional climate and the climatic future scenarios over northern South America.

In this work, we analyse the characteristics of the OLLJ at its active season (DJF) during warm (cold) phases of ENSO addressing the next questions: (a) Does ENSO modulate the frequency of occurrence of the OLLJ?; (b) How do wind speeds of the OLLJ change during ENSO?; (c) Does ENSO modulate moisture transport and precipitation along the OLLJ corridor? This work is organized as follows. Section 2 describes the datasets used. Section 3 describes the procedure to investigate the OLLJ in terms of the changes during the phases of ENSO of the NASH-NET gradient pressure, its frequency of occurrence, moisture transport by the OLLJ, and its vertical structure. The results and discussions are presented in section 4, and conclusions are drawn in section 5.

2 | DATA

- Oceanic Niño index (ONI): We use the ONI index, which is based on variations in 3-month running means of SSTs in a central Pacific region defined as Niño3.4 (NOAA, 2019a; NOAA, 2019b) above the +0.5°C (below −0.5°C) threshold to identify the El Niño (La Niña) events. The ONI index is available on the web page: https://origin.cpc.ncep.noaa.gov/products/analysis_monitoring/ensostuff/ONI_v5.php.
- ERA5 atmospheric reanalysis: We use data from the ERA5 atmospheric reanalysis (Hersbach *et al.*, 2019), which provides estimates of atmospheric, land, oceanic and climatic variables. The ERA5 data covers the Earth on a 30 km grid and it resolves the atmosphere using 137 levels, from the surface up to a height of 80 km. Here, we use the following variables: daily and hourly wind speed at pressure levels from 1,000 to 500 hPa, specific humidity, sea level pressure (SLP), and geopotential

height at 925 and 200 hPa. Furthermore, we calculate the water vapour flux (WVF) as the product between total wind speed and the specific humidity (Peixoto and Oort, 1993) $WVF = qV$ ($V = \sqrt{u^2 + v^2}$, where u and v are the zonal and meridional wind speeds).

- CHIRPS: We use data from Climate Hazards Group InfraRed Precipitation with Station data (CHIRPS), which is a high-resolution dataset (0.25°), at daily and monthly time scales in the quasi-global rainfall dataset (Funk *et al.*, 2015). CHIRPS data spans 50°S–50°N (and all longitudes) and ranges from 1981 to near-present. In this work, we use 0.25° spatial resolution and a daily time resolution from January 1, 1981 to December 31, 2020 over Northern South America (10°S–20°N and 85°–50°W).

3 | METHODS

3.1 | The NASH-NET pressure gradient associated with the OLLJ

We evaluated the pressure conditions during each ENSO phase by computing SLP anomaly fields as the difference between El Niño (La Niña) and neutral conditions in a region between 60°N–20°S and 120°W–10°E. Next, we quantified the SLP gradient between the NASH and NET regions to further study its relation with the OLLJ according to Vernekar *et al.* (2003). To that end, we identified the centre of the NASH as the region with the higher geopotential height at 850 hPa with a climatological mean area (20°–40°N, 80°–10°W) as proposed by Davis *et al.* (1997) and then we averaged the monthly SLP over that region. After that, we computed the SLP monthly mean in the NET region, which exhibits the lowest mean SLP over the northern Amazon (2°–3°S, 69°–70°W).

Furthermore, we calculate the NASH-NET gradient using the SLP standardized anomalies, which consist of subtracting to each month its corresponding long-term monthly mean and dividing it by its monthly standard deviation. Moreover, we calculated standardized anomalies of zonal wind speed at 925 hPa averaged over the OLLJ index area (6°–8°N and 67°–69°W), which was selected according to the recent work by Builes-Jaramillo *et al.* (2022). Finally, we calculated Pearson correlations between the centre of the NASH minus NET SLP gradient anomaly and the OLLJ wind speeds anomalies for each of the DJF months.

3.2 | The frequency of occurrence of the OLLJ

We use the criteria proposed by Jiménez-Sánchez *et al.* (2019) to identify the OLLJ frequency of occurrence,

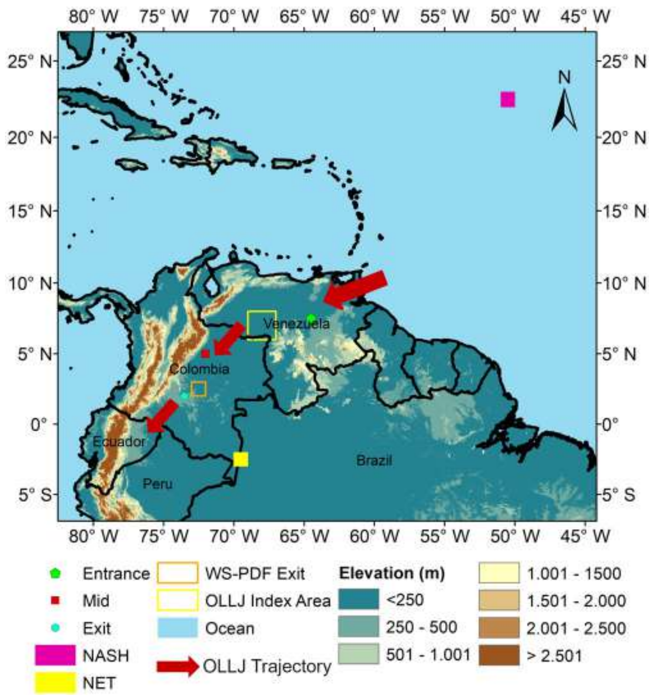

FIGURE 1 Study region with the location of the northern South America and tropical North Atlantic regions. (purple box) Center of the NASH and (yellow) NET regions. OLLJ corridor: Entrance (green), Mid (red), and Exit (blue) regions. The empty boxes indicate the regions where the probability density functions for the maximum wind speed are computed (WS-PDF) and OLLJ index area [Colour figure can be viewed at wileyonlinelibrary.com]

which are based on both Bonner (1968) and Ranjha *et al.* (2013). By these means we test that (a) maximum wind is within the lowest 2 km above ground level; (b) maximum wind speed is at least 40% higher than the one at the surface (1,000 hPa); and (c) the wind speed above the level of maximum wind decreases by at least 20% within 3 km (~700 hPa) of the surface.

We computed the wind speed for the study region (10°S–20°N and 85°–50°W) and tested these three conditions: grid cells that match the three conditions were flagged as 1, otherwise were flagged as 0. This calculation was done for hourly wind fields from 1979 to 2020 of December, January, and February at 1200 UTC (0700 LST), which is the hour with the higher frequency of occurrence of the OLLJ according to Jiménez-Sánchez *et al.* (2019) and Builes-Jaramillo *et al.* (2022). Hence, when 1 day at 1200 UTC is flagged as one is considered an OLLJ active day. Each month was previously classified according to the neutral conditions (that have been used as the reference) and the ENSO phases (El Niño or La Niña). Therefore, for each ENSO episode, the frequency of occurrence of the OLLJ was computed in each grid cell, the total OLLJ days were divided by the total number of days in the month. This calculation produces the frequency of occurrence that ranges from 0 to 100%.

3.3 | Diurnal variability during ENSO

We estimated the diurnal variability of wind speed during DJF. Three specific locations in the jet corridor were selected: entrance (7.5°N, 64.5°W), mid-region (5°N, 72°W), and exit (2°N, 73.5°W). For each location, we classified the months associated with Neutral conditions as well as for La Niña and El Niño phases. Then, we averaged all data at each hour of every day during the 1979–2020 period. Then, results for each location and ENSO phase were plotted in a pressure–time diagram.

On the other hand, we computed the Probability Density Functions (PDF) for the maximum wind speed during the OLLJ days at two regions: (a) the OLLJ index area (6°–8°N, 67°–69°W) and (b) an area near the exit location WS-PDF (2°S–3°N, 72°–73°W) (Figure 1). To evaluate the differences between PDFs we used the Kolmogorov–Smirnov test.

3.4 | Composite analysis

We use the composite analysis method to study the relationships between the activity of the jet during the ENSO phases and different climatic phenomena in the region of the OLLJ corridor (Terray *et al.*, 2003; Boschat *et al.*, 2016; Xie *et al.*, 2017). The general procedure summarizes as (a) we define the Neutral, the La Niña, and the El Niño dates using the ONI index; (b) we isolate the OLLJ days in the area of higher frequency of occurrence 6°S–8°N and 67°–69°W, these events constitute the key times; (c) we isolate variables (e.g., occurrences of OLLJ, the OLLJ wind speeds, WVF, precipitation, among others) corresponding to the OLLJ days during ENSO by calculating the average for all key times; and finally, (d) we use the test proposed by Terray *et al.* (2003) to verify whether there is a significant difference between the average for the phases of ENSO and the Neutral ones.

4 | RESULTS

4.1 | The NASH-NET pressure gradient associated with the OLLJ

Figure 2 shows the SLP anomaly fields for El Niño minus Neutral conditions (La Niña minus Neutral conditions) during the December, January and February. During El Niño (La Niña), the NASH region (20°–40°N, 80°–10°W) experiences a gradual reduction (increase) of the SLP anomalies up to 4.0 hPa (2.5 hPa) from December to February. Note that the higher differences occur during February in both ENSO phases. Furthermore, during El Niño (La Niña), the NET region exhibits a change of SLP over the northwestern Amazon region ranging between 1.0 and 0.0 hPa (0.0 and 1.0 hPa). In this sense, the SLP anomalies over the NASH region are higher than the SLP anomalies over the NET region, thus driving the SLP gradient over the region. Here, we hypothesize that such NASH-NET gradient could be related to the OLLJ wind speed.

Hence, in order to associate those processes, we quantify the Pearson correlation between the standardized NASH-NET SLP gradient and the OLLJ represented by the standardized mean wind speed over the OLLJ index area. Our results show a significant negative correlation ($r = -0.53$, p-value < 0.05) indicating that negative anomalies of wind speed (higher easterly wind speed) are associated with positive anomalies of SLP gradients (higher SLP gradients) (Figure 3). Thus, the previous result indicates that during La Niña (El Niño) is expected to find higher (lower) wind speeds in the OLLJ corridor during the DJF months.

4.2 | Vertical profiles of seasonal wind speed

Figure 4 shows the mean vertical profiles during the ENSO phases for each month of OLLJ activity, along with the three locations of the jet pathway (entrance, mid, and exit). The highest wind speeds were found in the entrance region at 900 hPa with values near 9 m·s^{-1} for January and February during both ENSO phases.

At the entrance region, the wind speed has similar magnitudes among the ENSO phases, while for mid and exit, the wind speed differences with the Neutral conditions are up to 2 m·s^{-1}. Mid and exit regions exhibit similar profiles during the 3 months; however, marked differences are observed among the ENSO phases during February (8 m·s^{-1} during La Niña and 5 m·s^{-1} during El Niño). In general, meridional wind speed decrease (increase) in mid and exit regions during El Niño (La Niña). These wind speed variations from the Neutral conditions are observed during December, January and February and persist in March (see Figure S1, Supporting Information). Interestingly, the peak winds are located at 900 hPa in the entrance and mid-region, while in the exit region, the peak winds lift to 850 hPa. These changes in the level of maximum wind speed obey topographic conditions: the OLLJ enters as zonal wind over the Venezuela plains, once it reaches the Andes mountain

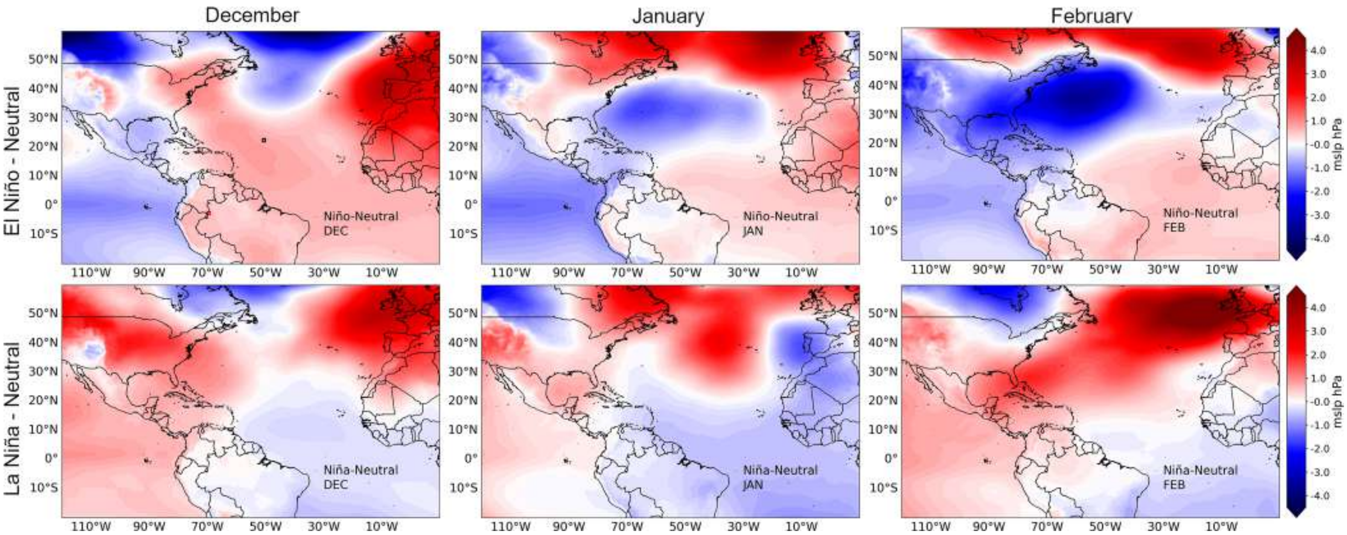

FIGURE 2 SLP anomaly fields (hPa) at El Niño/La Niña phases with respect to Neutral conditions during December, January and February [Colour figure can be viewed at wileyonlinelibrary.com]

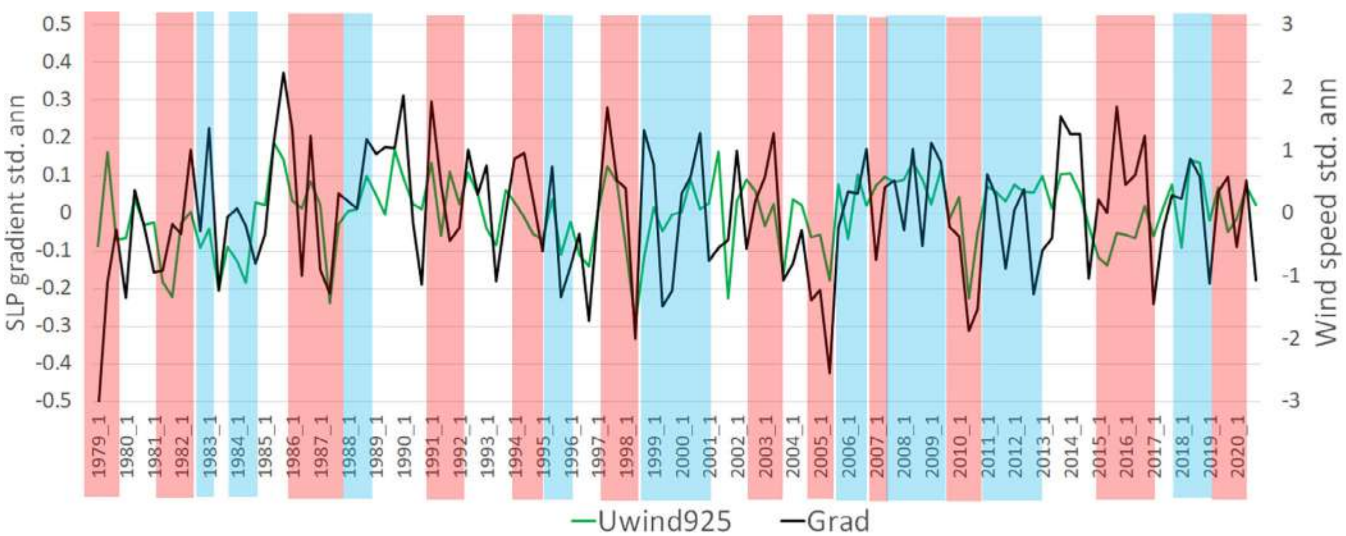

FIGURE 3 Standardized anomalies of u in 6°–8°N and 67°–69°W at 925 hPa and the NASH-NET SLP gradient during DJF. Pearson correlation coefficient $r = -0.53$. Blue shadow represents La Niña events and red shadow represent El Niño events [Colour figure can be viewed at wileyonlinelibrary.com]

range shifts southward where the flow deepens (between the 900–800 hPa) due to a Venturi effect (Jiménez-Sánchez *et al.*, 2020). Similarly, Jones (2019) also indicates the height of the northern branch of SALLJ around 850 hPa over locations near the entrance and exit regions.

4.3 | Frequency of occurrence of the OLLJ during ENSO

Figure 5 (upper row) shows the frequency of occurrence of the OLLJ at 1200 UTC (0700 LST) for the Neutral conditions during December, January, and February. It also shows the differences between El Niño (La Niña) and Neutral conditions during the 1979–2020 period (mid and bottom rows). One remarkable feature of the OLLJ during the Neutral conditions is that the region of the higher frequency of occurrence (>80%) remains located in the entrance region of the jet over central Venezuela (around 8°N and 67°W). Furthermore, there is a contrasting pattern of frequency of occurrence of the OLLJ during the ENSO phases between the entrance and mid-exit regions for December and January. In that sense, we found that the frequency of occurrence of the OLLJ in the mid and exit regions decreases during the El Niño

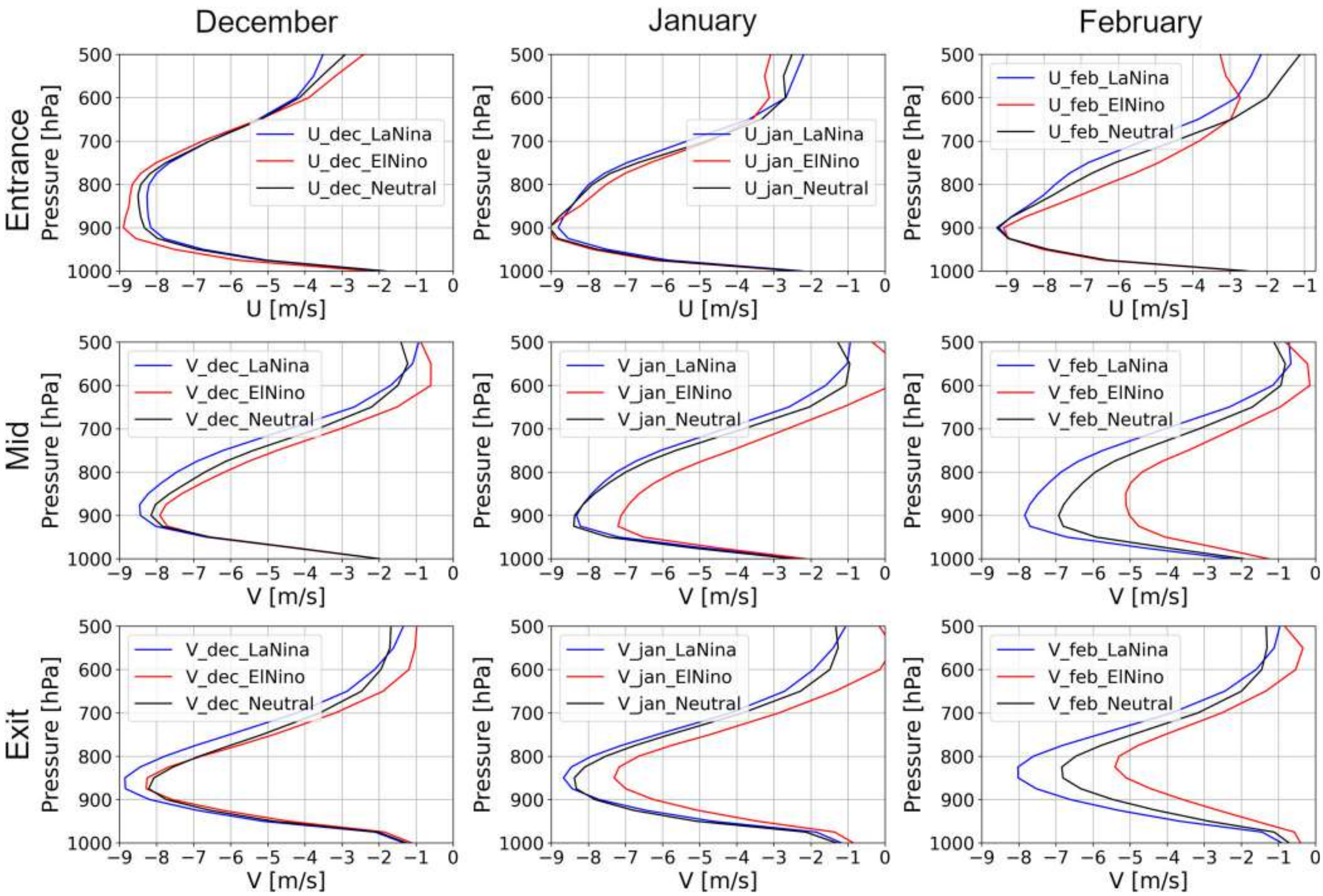

FIGURE 4 Mean vertical profiles of wind speed (m·s^{-1}) for the Neutral conditions and the phases of ENSO (El Niño and La Niña) during December, January, and February for the 1979–2020 period. The profiles are estimated in the following points along the pathway of the OLLJ: Entrance (7.5°N, 64.5°W) for the *u* component of wind, mid (5°N, 72°W) and exit (2°N, 73.5°W) for the v component of wind [Colour figure can be viewed at wileyonlinelibrary.com]

phase (Figure 5, middle row) between 5–24%, with the higher reduction in January over the Colombian east plains. Moreover, during this phase of ENSO, the frequency of occurrence increases between 5 and 10% at the entrance region of the jet (northwestern Venezuela), with statistically significant values during December and February. During La Niña (Figure 5, bottom row), the frequency of occurrence increases up 4–11% in the mid and exit regions during December and February, at the east Colombian plains and the borders between Colombia, Ecuador, and Peru, while at the entrance region of the OLLJ exhibits a decrease in the frequency of occurrence near to 10% in December and less than 4% in February. There are fewer observed changes in the frequency of occurrence and significance during La Niña. The influence of El Niño (La Niña) over the frequency of occurrence of the OLLJ spans even further the DJF months of the jet it extends until March as a generalized reduction (increase) in the jet corridor (see Figure S2).

Figure 6 shows the diurnal cycle of the wind speed cross-sections for El Niño and La Niña phases at the entrance, mid, and exit regions of the OLLJ corridor in February (December and January show similar features in Figures S3 and S4). In general, at the entrance region, the OLLJ showed the highest wind speeds (around 11 m·s^{-1}) from 2200 to 0700 LST at the pressure levels between 950–900 hPa during both ENSO phases. In the mid-region, the highest wind speeds (11 m·s^{-1}) occur between 0700 and 1000 LST around the pressure levels 925–850 hPa, while in the exit region, this feature is observed between 0800 and 1200 LST around the 850 hPa pressure level. In addition, a second night-time maximum (2200 LST) with values around 9 m·s^{-1} is observed during El Niño at the mid-region.

The OLLJ cross-sections show different features related to the ENSO phases along its pathway. At the entrance, differences are unclear between both phases of ENSO, except for a mid-troposphere extended core of maximum velocity (11 m·s^{-1}) that appears during El

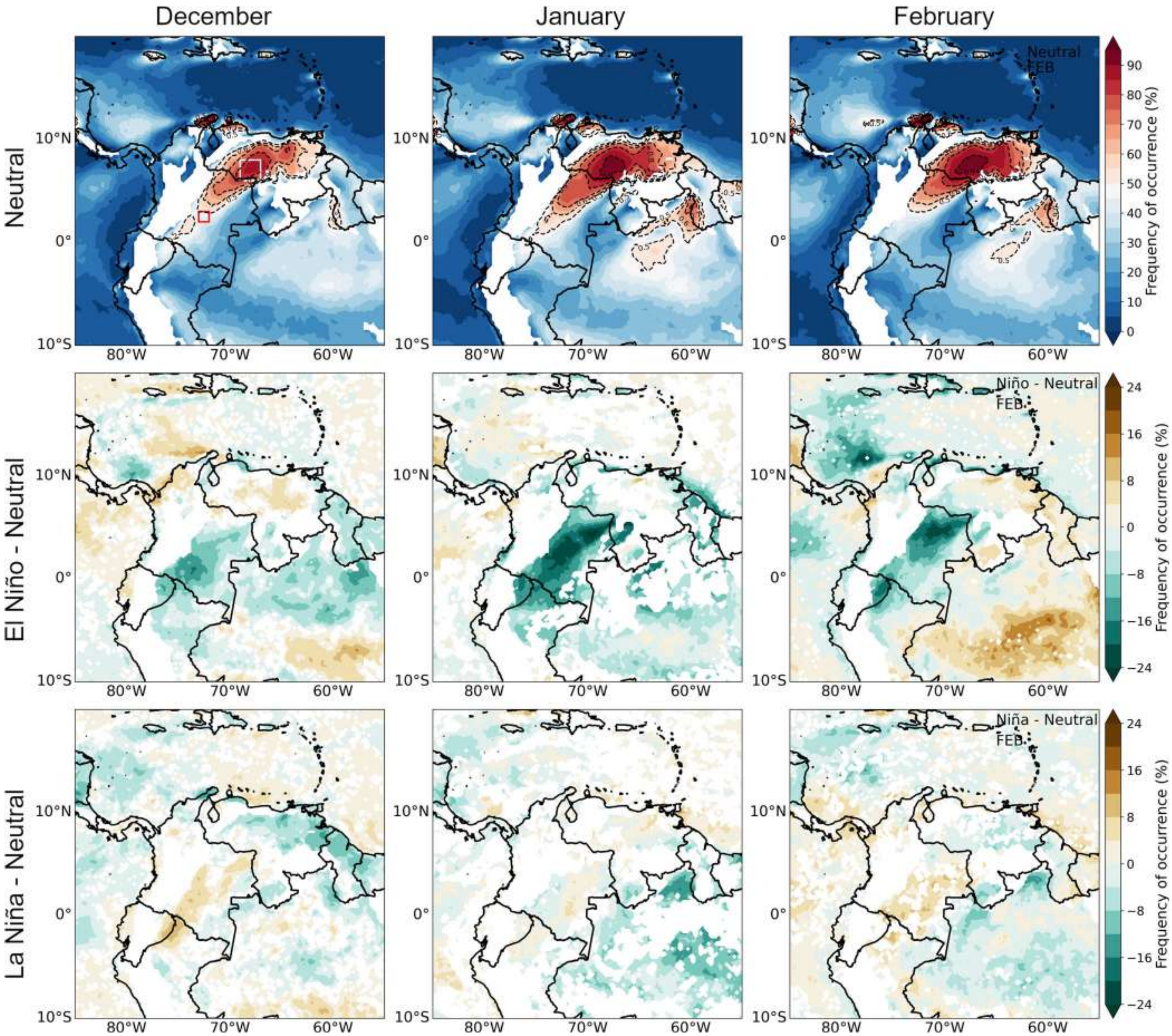

FIGURE 5 (top row) Frequency of occurrence (%) of the OLLJ using daily wind speed at 1200 UTC from 1979 to 2020. (middle row) Difference between El Niño and Neutral months frequency of simultaneous occurrence for the three criteria of OLLJ for wind speed at 1200 UTC from 1979 to 2020 for December, January, and February (left to right). (bottom row) As the previous one for La Niña. Contour lines are plotted for frequencies between 50 and 100%. White pixels depict grid points with no statistical significance according to the Terray test. White box (6°S–8°N and 67°–69°W) and red box (2°S–3°N and 72°–73°W) in the upper left panel depict the areas to compute the distribution of maximum wind speed [Colour figure can be viewed at wileyonlinelibrary.com]

Niño beyond 1000 LST. However, the cross-sections of the differences from the Neutral conditions (not shown) suggest an increase of wind speed during El Niño and a decrease during La Niña around 950 hPa, especially during December and January. In contrast, during La Niña (El Niño), wind speed increases (decreases) in agreement with the vertical profiles (Figure 4) and the frequency of occurrence over the mid and exit regions (Figure 5). Changes at these regions are at the pressure level of 850 hPa, which coincides with the South America low-level jet (SALLJ). These contrasting relationships along the OLLJ corridor suggest different mechanisms driving the wind speed of the OLLJ during both ENSO phases. Our results agree with those described by Jiménez-Sánchez *et al.* (2020) which evidenced the hours of maximum wind speed of the OLLJ between 0400 and 0900 LST depending upon the region. The wind speed patterns previously described for both ENSO phases are observed during December and January along the OLLJ corridor (see Figures S3 and S4).

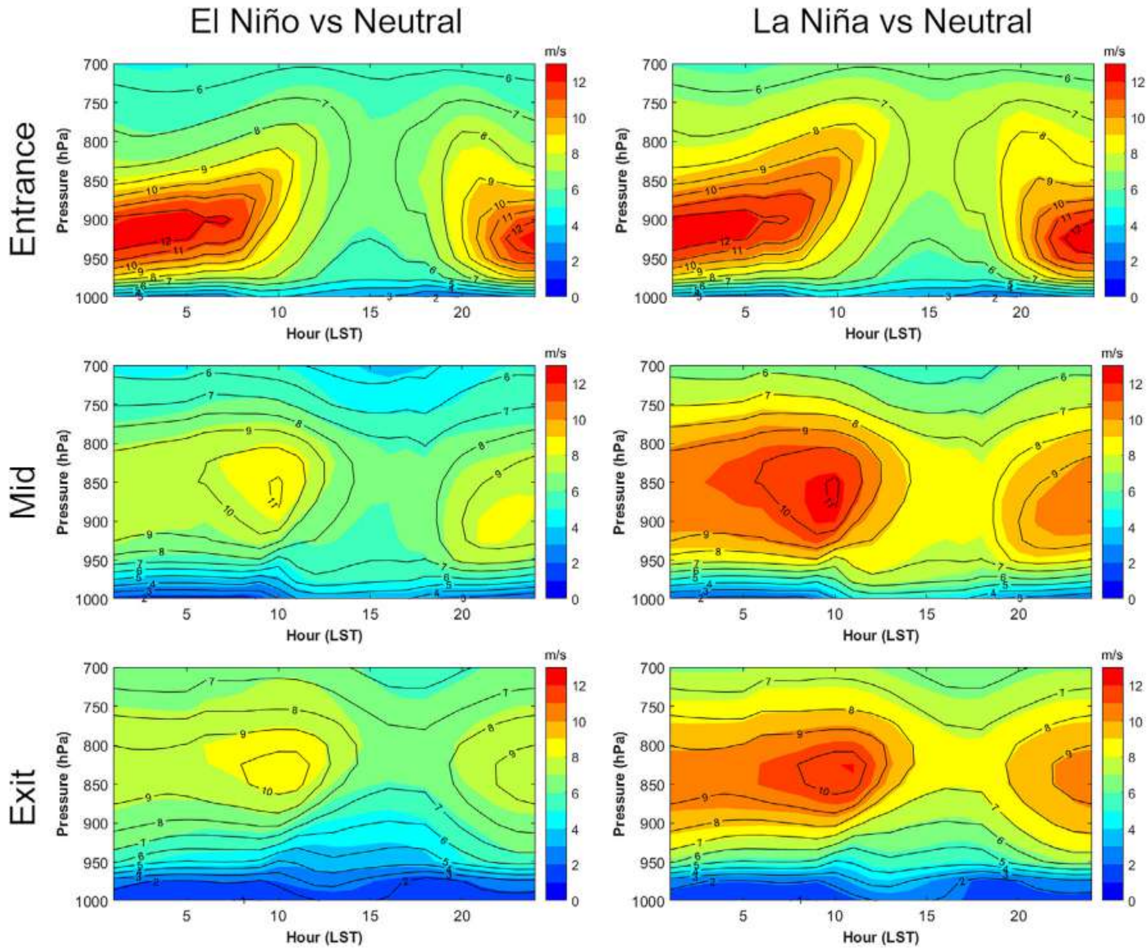

FIGURE 6 Diurnal cycle of the February wind speed ($m \cdot s^{-1}$) cross-sections during El Niño (La Niña) phases (filled contours) and Neutral conditions (black contours). Climatology between 1979 and 2020. Profiles are defined for the entrance (7.5°N, 64.5°W), mid (5°N, 72°N), and exit regions (2°N, 73.5°W) [Colour figure can be viewed at wileyonlinelibrary.com]

Figure 7 shows the probability density functions (PDFs) of the maximum wind speed during the Neutral conditions as well as for El Niño and La Niña in the OLLJ days, for two areas: (a) the OLLJ index area (Figure 7a–c) defined at coordinates: 6°S–8°N, 67°–69°W and (b) the exit region (Figures 1 and 7d–f WS-PDF exit) at 2°S–3°N, 72°–73°W. In general, PDFs show maximum wind speeds around 10–15 $m \cdot s^{-1}$. During El Niño, the PDF shifts to the left side, which is more evident across the advance of the season. This result evidence lower (higher) wind speed during El Niño (La Niña). In particular, the wind speed exhibits its highest differences in February. Our results show that maximum wind speeds during the occurrence of the OLLJ exceed 10 $m \cdot s^{-1}$, in agreement with those results found by Jones (2019) for the northern South America branch of the SALLJ. Notwithstanding, we found a statistically significant difference according to the Kolmogorov–Smirnov test among the wind speeds during the phases of ENSO.

Figure 8 shows the composites of geopotential height anomalies and wind speed fields at 925 hPa during the OLLJ active days for both ENSO phases. In general, composites do not exhibit significant changes from Figure 2 and evidence contrasting changes in the meridional patterns between the NASH and NET regions. During El Niño, NASH experiences changes in geopotential height because negative geopotential height anomalies (around 15 m) move from the North Atlantic Ocean (December) towards North America (February). During La Niña, NASH exhibits geopotential height anomalies that start with a dipole in December, and then it shifts to positive anomalies for January and February. Note that the highest positive anomalies occur during February with values up to 30 m (above Neutral conditions). Meanwhile, northern South America (including NET) shows negligible geopotential height anomalies predominate during all months. In general, during El Niño (La Niña), NASH experiences negative (positive) pressure anomalies while NET experiences positive (negative) ones. Then,

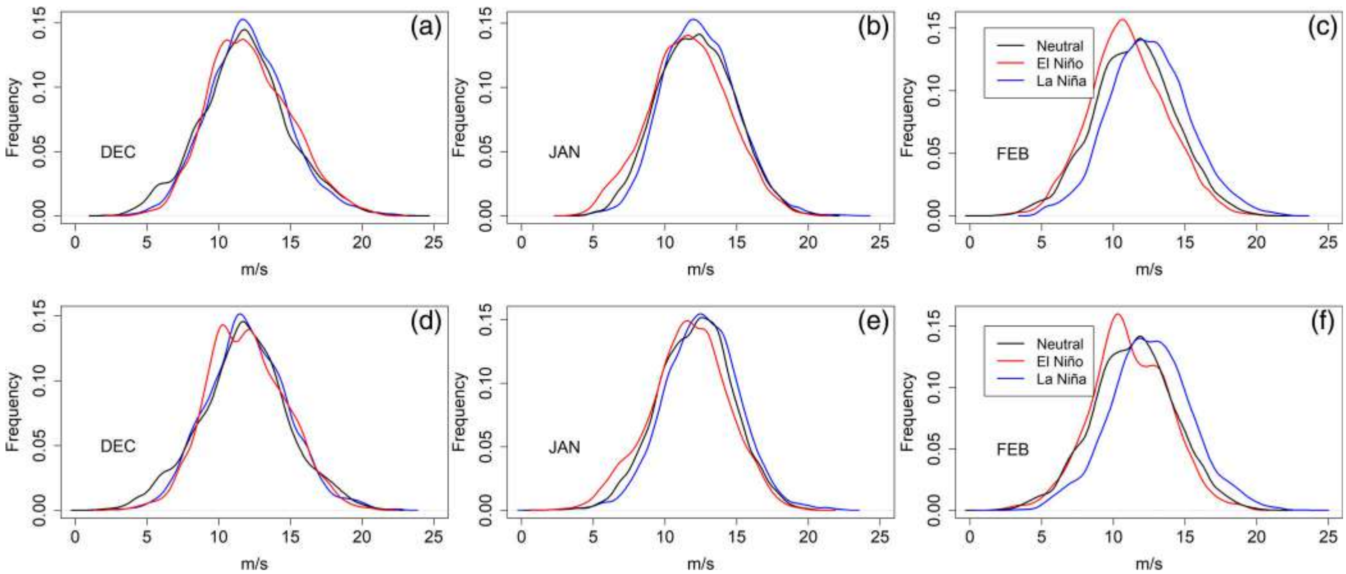

FIGURE 7 Probability density functions of the maximum wind speed during the OLLJ days in the DJF months over the OLLJ index area at 6°S–8°N and 67°–69°W (upper row) and over the WS-PDF exit area 2°S–3°N and 72°–73°W (bottom row). All distributions are statistically different according to the Kolmogorov–Smirnov test of equal distributions [Colour figure can be viewed at wileyonlinelibrary.com]

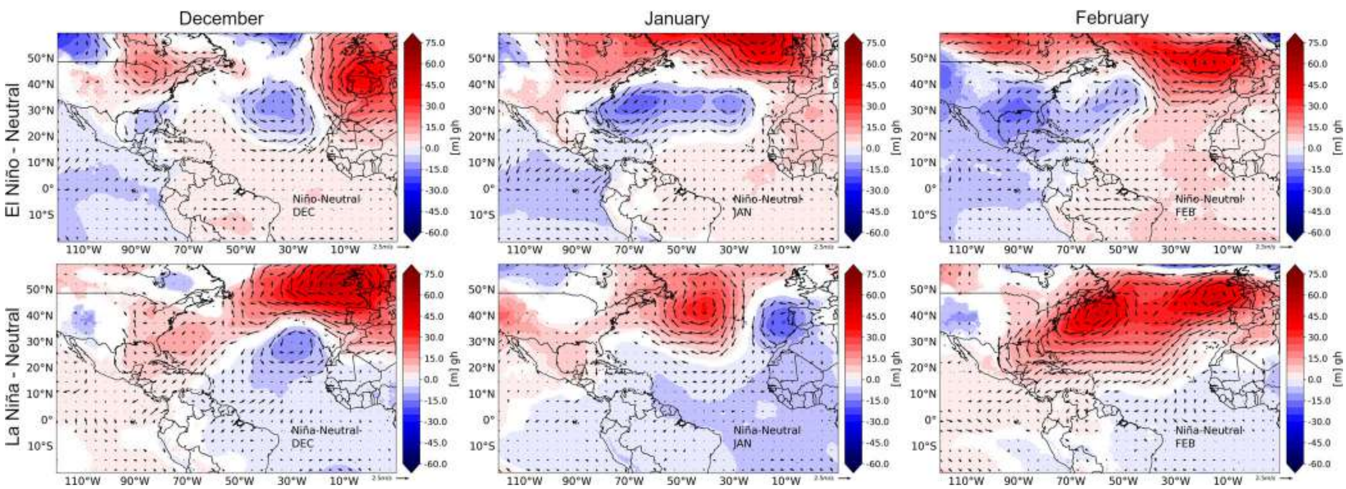

FIGURE 8 Geopotential height (m) and wind vector anomalies composites for active OLLJ days during December, January, and February for El Niño (La Niña) minus Neutral conditions at 925 hPa. White pixels depict grid points with no statistical significance according to the test developed by Terray *et al.* (2003) [Colour figure can be viewed at wileyonlinelibrary.com]

although there are no significant changes over NET, the pressure gradient between NASH and NET tends to decrease (increase) during El Niño (La Niña). Hence, this gradient might induce lower (higher) winds during El Niño (La Niña) as the ones evidenced in Figure 8, top row (Figure 8, bottom row). Those results are consistent with those shown in the vertical profiles (Figure 4) and the frequency of occurrence of the OLLJ (Figure 5). Moreover, Figure 8 shows no-significant areas in the mid and exit regions of the OLLJ during El Niño (La Niña) in February (December).

4.4 | The OLLJ and its relationship with moisture transport and precipitation in the region

We analysed the moisture transport and precipitation during the phases of ENSO. During OLLJ days in the Neutral conditions are found the highest values of water vapour flux (WVF) (Figure 9, top row) are found over the Caribbean Sea (up to 180 $g \cdot m^{-1} \cdot kg \cdot s^{-1}$), the Panama gap flow, the Guyanas LLJ, and the OLLJ corridor (the last three places exhibiting values of WVF up to

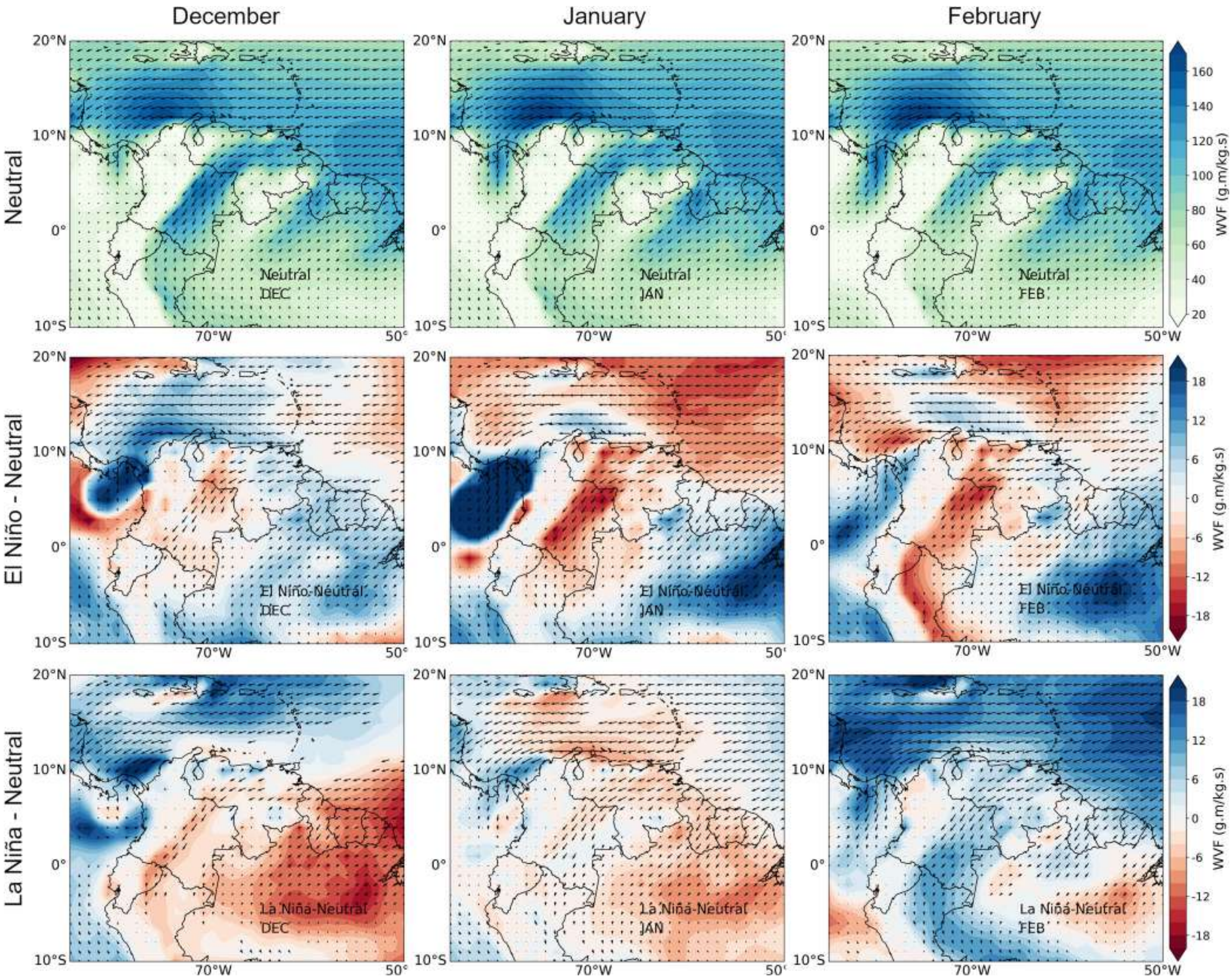

FIGURE 9 (top row) Composite of water vapour flux (WVF; $g \cdot m^{-1} \cdot kg \cdot s^{-1}$) and wind speed vectors at 925 hPa during active OLLJ days in the Neutral conditions. (mid row) Difference between water vapour flux (WVF) during active OLLJ days in the El Niño and Neutral conditions. (vectors) Composites of wind speed during active OLLJ days at 925 hPa in El Niño. (bottom row) WVF during the active OLLJ days in La Niña subtracting the WVF during the Neutral conditions. (vectors) Composites of wind speed at 925 hPa during the OLLJ active days in La Niña subtracting the WVF in the Neutral conditions. Winds at the 925 hPa pressure level are plotted where the WVF differences are statistically significant according to the test developed by Terray *et al.* (2003) [Colour figure can be viewed at wileyonlinelibrary.com]

140 $g \cdot m^{-1} \cdot kg \cdot s^{-1}$). We also computed the WVF difference between OLLJ days during the El Niño and Neutral conditions (Figure 9, middle row), which shows a reduction from December to February in a range from 10 to 18 $g \cdot m^{-1} \cdot kg \cdot s^{-1}$. The WVF reduction along the OLLJ pathway is higher in February, reaching beyond the exit region of the jet down to Peru. In contrast, the Panama gap flow and the Guyana LLJ areas exhibit an increased WVF of 18 and 6 $g \cdot m^{-1} \cdot kg \cdot s^{-1}$, respectively. During the OLLJ days in the La Niña phase, the WVF also decreases during December–January (6–12 $g \cdot m^{-1} \cdot kg \cdot s^{-1}$), whereas during February increases over the jet corridor (up to 10 $g \cdot m^{-1} \cdot kg \cdot s^{-1}$). In contrast, the integrated vapour transport (IVT) composites provided by Montini *et al.* (2019) suggest that this variable does not change during El Niño and La Niña over the OLLJ corridor. However, Montini *et al.* (2019) highlighted an increase of IVT over northern Brazil during that phase of ENSO, a feature also found in our WVF composites (Figure 9, middle row). Our results emphasize February as the month with a consolidated change in WVF along the OLLJ corridor, indicating the enhanced activity of ENSO in the January–March period, also observed in the frequency of occurrence of the OLLJ (see Figure S2).

Figure 10 precipitation over the continent during active days of the OLLJ for the Neutral conditions (upper row) and precipitation anomalies during each phase of ENSO (middle and bottom rows). The location of the

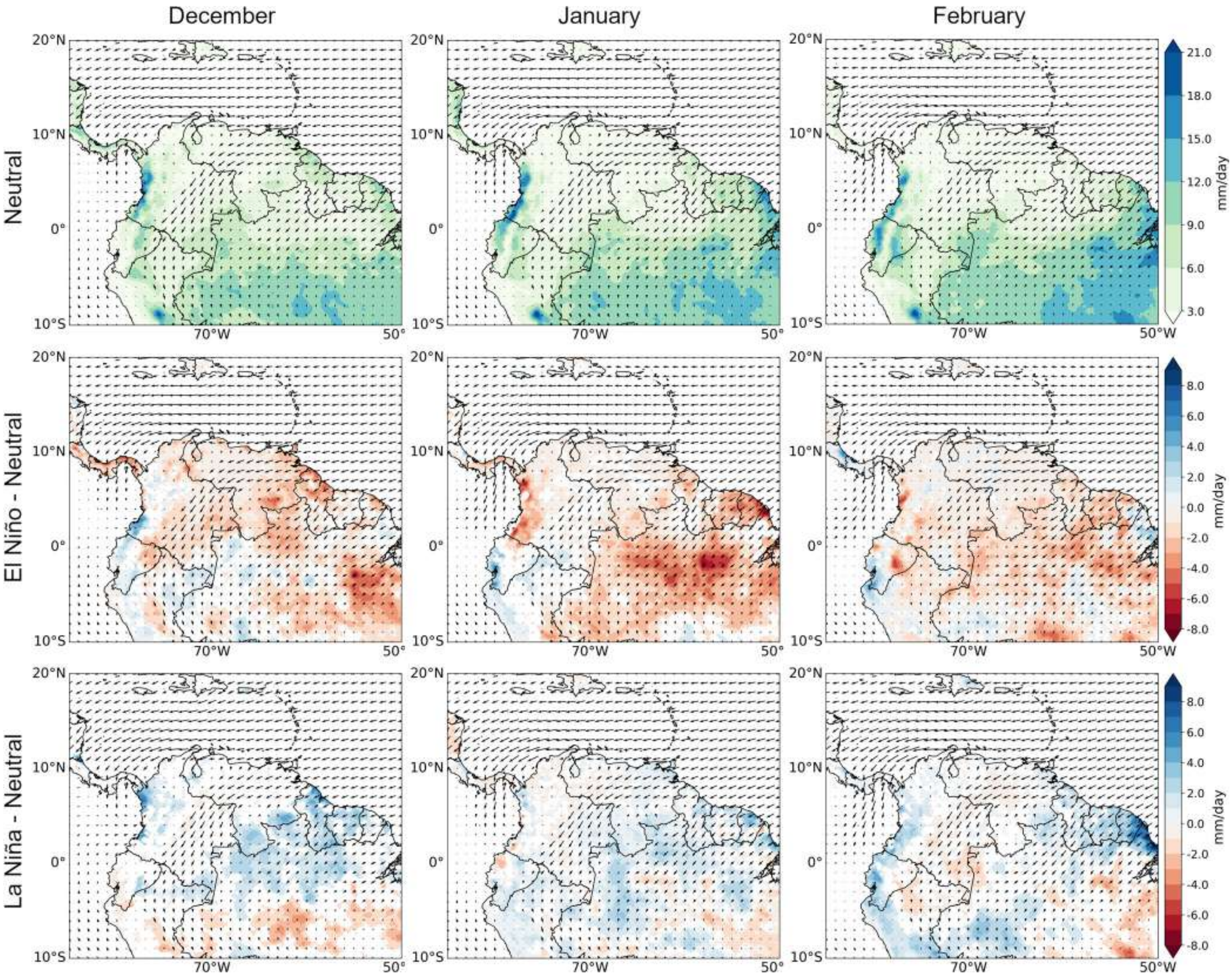

FIGURE 10 (upper row) Precipitation (mm·day^{-1}) during the active days of OLLJ in the Neutral conditions for the months December, January, and February. Precipitation anomalies (mm/day) between El Niño (La Niña) and Neutral conditions (mid and bottom row). (vectors) Composite of wind speeds at 925 hPa during Neutral, El Niño, and La Niña, respectively. White pixels depict grid points with no statistical significance according to the test developed by Terray *et al.* (2003) [Colour figure can be viewed at wileyonlinelibrary.com]

higher values of precipitation is further south, owing to the seasonal migration of the ZCIT (Berry and Reeder, 2014). This figure highlights the lower values of precipitation along the OLLJ corridor during DJF as reported previously (Labar *et al.*, 2005; Builes-Jaramillo *et al.*, 2022). Figure 10 (middle and bottom rows) also shows the differences from Neutral conditions between precipitation for each month in the active OLLJ season during El Niño and La Niña with respect to the Neutral conditions, respectively. Meanwhile, notable changes occur further south, precipitation exhibits the lowest values in the OLLJ corridor (around 2 mm·day^{-1}) during the months of the higher frequency of occurrence of the OLLJ (Figure 10, upper row). Therefore, the El Niño – Neutral differences fields (Figure 10, middle row) exhibits a reduction up to 2.0 mm·day^{-1} for December and February, whereas the La Niña – Neutral difference shows no reduction during December and January, and a reduction with values lower than 2 mm·day^{-1} along the OLLJ pathway in February. Hence there is a mild reduction in precipitation during both ENSO phases. Accumulated precipitation during the DJF months exhibits reduction for both ENSO phases reaching values up to 6 mm·day^{-1} during El Niño and 2 mm·day^{-1} during La Niña (see Figure S5).

5 | CONCLUSIONS AND FUTURE WORK

We studied the Orinoco low-level jet (OLLJ) during its most active season (December–January–February) and the canonical phases of ENSO (El Niño and La Niña). Our results suggest that ENSO phases modulate the OLLJ with significant changes between the entrance, the mid, and exit regions along the jet pathway.

Regionally, during El Niño (La Niña), negative (positive) anomalies over the NASH region might induce lower (higher) surface pressure gradient between the North Atlantic subtropical high and the near-equatorial trough (NASH-NET SLP gradient). Associated with this, the wind maxima decrease (increase) up to -2 m·s^{-1} (up to 1 m·s^{-1}) during El Niño (La Niña) over the mid and exit regions. In addition, the height of the maximum wind speed varies along the OLLJ pathway: at the entrance, zonal winds are located around 900 hPa, and downstream, meridional winds deepen reaching up 850 hPa. This shift in the OLLJ height has been explained by a Venturi effect of the Andes mountain range that changes the zonal winds into meridional ones (Jiménez-Sánchez *et al*., 2020).

The frequency of occurrence of the OLLJ was examined during the phases of ENSO, exhibiting significant changes during El Niño, especially over the Colombian east plains. One notable feature is that the frequency of occurrence changes during El Niño (La Niña) along the OLLJ pathway with an increase (reduction) of the OLLJ days over the entrance (mid-to-exit) region. In particular, during El Niño in January, the OLLJ exhibits its highest reduction in the frequency of occurrence, with changes up to 24% in the eastern Colombian plains. During La Niña, there is a significant increase in the frequency of occurrence around 6–16% in the eastern Colombian plains and the border with Ecuador and Peru. These results are supported by the PDFs of the maximum wind speed during OLLJ days, which show statistical difference in the distributions for each ENSO phase. In this sense, Jones (2019) did not find significant changes in the winds of the northern branch of the SALLJ (which includes the OLLJ corridor) during ENSO. We argue that the absence of a clear difference during the ENSO phases obeys different approaches between the mentioned work by Jones (2019) and our study. First, instead of using the criteria proposed by Montini *et al*. (2019) for identifying the jet occurrences, we used the criteria proposed by Jiménez-Sánchez *et al*. (2019). Second, the hour of evaluation of the events by Jones (2019) was the mean between 0000 UTC and 0600 UTC while ours was 1200 UTC according to previous studies.

The diurnal cycle of the OLLJ winds remains consistent with previous work. In agreement with Jiménez-Sánchez *et al*. (2020), it shows a wind maximum near midnight (local hour) at the entrance and the advance of this maximum around 0800–1000 LST over the mid and exit regions. The previous result is valid for both phases of ENSO, without changes in the timing of the diurnal cycle that can be associated with ENSO. However, the intensity of the jet winds increases (decreases) with La Niña (El Niño) in accordance with the vertical profiles.

Results show consistent atmospheric pressure patterns that change with the phase of ENSO during the OLLJ days. In general, there are opposite pressure anomalies between NASH and NET regions. During El Niño (La Niña), lower (higher) pressure over NASH and higher (lower) pressure over NET induce a decrease (increase) in the pressure gradient in both regions, which in turn, would be related to lower (higher) wind speed anomalies over the OLLJ region. Moreover, for both phases of ENSO, we found that the wind speed and SPL patterns are consistent with those observed during the OLLJ days.

Our results evidence that the OLLJ general features of moisture transport remain consistent with the previous literature (Bovolo *et al*., 2018; Algarra *et al*., 2019; Jones, 2019; Montini *et al*., 2019; Builes-Jaramillo *et al*., 2022). Algarra *et al*. (2019) and Builes-Jaramillo *et al*. (2022) showed that the active period of the OLLJ (DJF) coincides with the dry season over the Orinoco region and the OLLJ transports moisture along the OLLJ corridor that sinks further south. Here, we extended the analysis under the different phases of ENSO. In particular, the water vapour flux (WVF) gradually decreases through the season, exhibiting the same pattern for both ENSO phases. Furthermore, we point out that during La Niña, February shows an interesting increase in the frequency of occurrence of OLLJ, higher wind speed, and an increase of the moisture transport, especially further south (Figure 9), which coincides with the reduction of precipitation in the OLLJ corridor (Figure 10). This result shows new insights regarding the moisture transport changes through the OLLJ corridor over Amazonia and northern Brazil, which reduces during both phases of ENSO, being higher during El Niño up 18 g·m^{-1}·kg·s^{-1}. Notwithstanding, precipitation shows a reduction in the OLLJ corridor with values around ±2–5 mm·day^{-1} during both phases of ENSO. Although there is no clear pattern of precipitation during ENSO over the study region, Jones (2019) states that the active northern branch of the SALLJ contributes to increasing precipitation in Bolivia. Hence, the modulation of precipitation due to OLLJ in zones further south of the region of study during ENSO deserves further research.

Further questions about the OLLJ and its regional and local characteristics during ENSO deserves future work: How is the influence of the Central or Eastern Pacific ENSO (Ashok *et al*., 2007; Timmermann *et al*., 2018) on the jet?; How is the jet modulated by the Atlantic El Niño events (Martín-Rey *et al*., 2014; Jia *et al*., 2019)?; Do CMIP climate models properly represent the OLLJ features?; Is the OLLJ, the northern branch of the SALLJ or is it an independent climatic feature?; How the water vapour flux transported by the OLLJ could be modulated by changes in the corridor land use? Tackling these questions would contribute for a better understanding of this Northern South America climate feature and in turn contribute to reducing uncertainties in global climate modelling.

AUTHOR CONTRIBUTIONS

Alejandro Builes-Jaramillo: Conceptualization; data curation; formal analysis; funding acquisition; investigation; methodology; project administration; resources; software; supervision; validation; visualization; writing – original draft; writing – review and editing. **Johanna Yepes:** Conceptualization; data curation; formal analysis; funding acquisition; investigation; methodology; resources; software; supervision; validation; visualization; writing – original draft; writing – review and editing. **Hernán D. Salas:** Conceptualization; data curation; formal analysis; funding acquisition; investigation; methodology; resources; software; supervision; validation; visualization; writing – original draft; writing – review and editing.

ACKNOWLEDGEMENTS

The work of A. Builes-Jaramillo is supported by Institución Universitaria Colegio Mayor de Antioquia. The work by H. D. Salas is supported by Institución Universitaria Colegio Mayor de Antioquia and by COLCIENCIAS – Grant for National Doctorates 617-2 (2013). The work by J. Yepes is supported by the project “El Chorro de los Andes Orientales –CHAO– y su relación con la hidro-climatología de Colombia.” ERA5 Reanalysis data is available at the European Copernicus Programme website (https://www.copernicus.eu/). The CHIRPS precipitation dataset is available at the University of California Santa Barbara Climate Hazards Center website (https://www.chc.ucsb.edu/data). The ONI index is available at the web-page: https://origin.cpc.ncep.noaa.gov/products/analysis_monitoring/ensostuff/ONI_v5.php.

ORCID

Alejandro Builes-Jaramillo https://orcid.org/0000-0002-3474-6922

REFERENCES

Agudelo, J., Arias, P.A., Vieira, S.C. and Martínez, J.A. (2019) Influence of longer dry seasons in the southern Amazon on patterns of water vapor transport over northern South America and the Caribbean. *Climate Dynamics*, 52, 2647–2665. https://doi.org/10.1007/S00382-018-4285-1.

Algarra, I., Eiras-Barca, J., Nieto, R. and Gimeno, L. (2019) Global climatology of nocturnal low-level jets and associated moisture sources and sinks. *Atmospheric Research*, 229, 39–59. https://doi.org/10.1016/j.atmosres.2019.06.016.

Amador, J.A. (2008) The intra-Americas sea low-level jet: overview and future research. *Annals of the New York Academy of Sciences*, 1146, 153–188. https://doi.org/10.1196/annals.1446.012.

Amador, J.A., Durán-Quesada, A.M., Rivera, E.R., Mora, G., Sáenz, F., Calderón, B. and Mora, N. (2016) The easternmost tropical Pacific. Part II: seasonal and intraseasonal modes of atmospheric variability. *Revista de Biología Tropical*, 64, 23. https://doi.org/10.15517/rbt.v64i1.23409.

Ashok, K., Behera, S.K., Rao, S.A., Weng, H. and Yamagata, T. (2007) El Niño Modoki and its possible teleconnection. *Journal of Geophysical Research*, 112, C11007. https://doi.org/10.1029/2006JC003798.

Berry, G. and Reeder, M.J. (2014) Objective identification of the intertropical convergence zone: climatology and trends from the ERA-Interim. *Journal of Climate*, 27, 1894–1909. https://doi.org/10.1175/JCLI-D-13-00339.1.

Bonner, W.D. (1968) Climatology of the low level jet. *Monthly Weather Review*, 96, 833–850. https://doi.org/10.1175/1520-0493(1968)096<0833:COTLLJ>2.0.CO;2.

Boschat, G., Simmonds, I., Purich, A., Cowan, T. and Pezza, A.B. (2016) On the use of composite analyses to form physical hypotheses: An example from heat wave–SST associations. *Scientific Reports*, 6, 1–10. https://doi.org/10.1038/srep29599.

Bovolo, C.I., Wagner, T., Parkin, G., Hein-Griggs, D., Pereira, R. and Jones, R. (2018) The Guiana Shield rainforests-overlooked guardians of South American climate. *Environmental Research Letters*, 13, 074029. https://doi.org/10.1088/1748-9326/aacf60.

Builes-Jaramillo, A., Yepes, J. and Salas, H.D. (2022) The Orinoco low-level jet and its association with the hydroclimatology of northern South America. *Journal of Hydrometeorology*, 23(2), 209–223. https://doi.org/10.1175/JHM-D-21-0073.1.

Davis, R.E., Hayden, B.P., Gay, D.A., Phillips, W.L. and Jones, G.V. (1997) The North Atlantic subtropical anticyclone. *Journal of Climate*, 10, 728–744. https://doi.org/10.1175/1520-0442(1997)010<0728:TNASA>2.0.CO;2.

Durán-Quesada, A.M., Sorí, R., Ordoñez, P. and Gimeno, L. (2020) Climate perspectives in the Intra-Americas seas. *Atmosphere*, 11, 1–32. https://doi.org/10.3390/ATMOS11090959.

Enfield, D.B. and Mayer, D.a. (1997) Tropical Atlantic sea surface temperature variability and its relation to El Niño–Southern Oscillation. *Journal of Geophysical Research*, 102, 929–945.

Enfield, D.B., Mestas-Nuñez, A.M., Mayer, D.A. and Cid-Serrano, L. (1999) How ubiquitous is the dipole relationship in tropical Atlantic sea surface temperatures? *Journal of Geophysical Research*, 104, 7841–7848. https://doi.org/10.1029/1998JC900109.

Espinoza, J.C., Garreaud, R., Poveda, G., Arias, P.A., Molina-Carpio, J., Masiokas, M., Viale, M. and Scaff, L. (2020) Hydroclimate of the Andes Part I: Main climatic features. *Frontiers in Earth Science*, 8, 1–20. https://doi.org/10.3389/feart.2020.00064.

Funk, C., Peterson, P., Landsfeld, M., Pedreros, D., Verdin, J., Shukla, S., Husak, G., Rowland, J., Harrison, L., Hoell, A. and Michaelsen, J. (2015) The climate hazards infrared precipitation with stations—a new environmental record for monitoring extremes. *Scientific Data*, 2, 21. https://doi.org/10.1038/sdata.2015.66.

García-Martínez, I.M. and Bollasina, M.A. (2020) Sub-monthly evolution of the Caribbean low-level jet and its relationship with regional precipitation and atmospheric circulation. *Climate Dynamics*, 54, 4423–4440. https://doi.org/10.1007/s00382-020-05237-y.

Gimeno, L., Dominguez, F., Nieto, R., Trigo, R., Drumond, A., Reason, C.J.C., Taschetto, A.S., Ramos, A.M., Kumar, R. and Marengo, J. (2016) Major mechanisms of atmospheric moisture transport and their role in extreme precipitation events. *Annual Review of Environment and Resources*, 41, 117–141. https://doi.org/10.1146/annurev-environ-110615-085558.

Hersbach, H., Bell, B., Berrisford, P., Horányi, A., Sabater, J.M., Nicolas, J., Radu, R., Schepers, D., Simmons, A., Soci, C. and Dee, D. (2019) Global reanalysis: goodbye ERA-Interim, hello ERA5. *ECMWF Newsletter*, 159, 17–24. https://doi.org/10.21957/vf291hehd7.

Jia, F., Cai, W., Wu, L., Gan, B., Wang, G., Kucharski, F., Chang, P. and Keenlyside, N. (2019) Weakening Atlantic Niño–Pacific connection under greenhouse warming. *Science Advances*, 5, eaax4111. https://doi.org/10.1126/sciadv.aax4111.

Jiménez-Sánchez, G., Markowski, P.M., Jewtoukoff, V., Young, G.S. and Stensrud, D.J. (2019) The Orinoco low-level jet: an investigation of its characteristics and evolution using the WRF model. *Journal of Geophysical Research: Atmospheres*, 124, 10696–10711. https://doi.org/10.1029/2019JD030934.

Jiménez-Sánchez, G., Markowski, P.M., Young, G.S. and Stensrud, D.J. (2020) The Orinoco low-level jet: an investigation of its mechanisms of formation using the WRF model. *Journal of Geophysical Research: Atmospheres*, 125, 1–23. https://doi.org/10.1029/2020jd032810.

Jones, C. (2019) Recent changes in the South America low-level jet. *npj Climate and Atmospheric Science*, 2, 1–8. https://doi.org/10.1038/s41612-019-0077-5.

Labar, R. J., Douglas, M., Murillo, J. and Mejia, J. F. (2005) The Llanos low-level jet and its association with Venezuelan convective precipitation.

Martín-Rey, M., Rodríguez-Fonseca, B., Polo, I. and Kucharski, F. (2014) On the Atlantic–Pacific Niños connection: a multidecadal modulated mode. *Climate Dynamics*, 43, 3163–3178. https://doi.org/10.1007/s00382-014-2305-3.

Montini, T.L., Jones, C. and Carvalho, L.M.V. (2019) The South American low-level jet: a new climatology, variability, and changes. *Journal of Geophysical Research: Atmospheres*, 124, 1200–1218. https://doi.org/10.1029/2018JD029634.

Montoya, G., Pelkowski, J. and Eslava, J. (2001) Sobre los vientos alisios del nordeste y la existencia de una corriente en el piedemonte oriental andino. *Revista de la Academia Colombiana de Ciencias*, 25, 363–370.

NOAA. (2019a) *Nino regions*. National Oceanic and Atmospheric Administration. https://www.cpc.ncep.noaa.gov/products/analysis_monitoring/ensostuff/nino_regions.shtml.

NOAA. (2019b) *Cold and warm episodes by season*. National Oceanic and Atmospheric Administration. https://origin.cpc.ncep.noaa.gov/products/analysis_monitoring/ensostuff/ONI_v5.php.

Peixoto, J., Oort, A., 1993. *Physics of Climate*. New York, Berlin, Heidelberg: Springer-Verlag.

Poveda, G., Álvarez, D.M. and Rueda, O.A. (2011) Hydro-climatic variability over the Andes of Colombia associated with ENSO: a review of climatic processes and their impact on one of the Earth's most important biodiversity hotspots. *Climate Dynamics*, 36, 2233–2249. https://doi.org/10.1007/s00382-010-0931-y.

Poveda, G. and Mesa, O.J. (2000) On the existence of Lloró (the rainiest locality on Earth): enhanced ocean–land–atmosphere interaction by a low-level jet. *Geophysical Research Letters*, 27, 1675–1678. https://doi.org/10.1029/1999GL006091.

Ranjha, R., Svensson, G., Tjernström, M. and Semedo, A. (2013) Global distribution and seasonal variability of coastal low-level jets derived from ERA-Interim reanalysis. *Tellus A: Dynamic Meteorology and Oceanography*, 65, 20412. https://doi.org/10.3402/tellusa.v65i0.20412.

Rodríguez-Gómez, C., Echeverry, G., Jaramillo, A. and Ladino, L.A. (2021) The negative impact of biomass burning and the Orinoco low-level jet on the air quality of the Orinoco River basin. *Atmósfera*, 497-520. https://doi.org/10.20937/ATM.52979.

Rueda, C. (2014) *Caracterización de la Corriente en Chorro de Bajo Nivel de los Llanos Orientales Colombianos*. Master's thesis, Universidad Nacional de Colombia.

Ruiz-Vásquez, M., Arias, P.A., Martínez, J.A. and Espinoza, J.C. (2020) Effects of Amazon basin deforestation on regional atmospheric circulation and water vapor transport towards tropical South America. *Climate Dynamics*, 54, 4169–4189. https://doi.org/10.1007/s00382-020-05223-4.

Salas, H.D., Poveda, G., Mesa, O.J. and Marwan, N. (2020) Generalized synchronization between ENSO and hydrological variables in Colombia: a recurrence quantification approach. *Frontiers in Applied Mathematics and Statistics*, 6, 3. https://doi.org/10.3389/fams.2020.00003.

Serna, L.M., Arias, P.A. and Vieira, S.C. (2018) Las corrientes superficiales de chorro del Chocó y el Caribe durante los eventos de El Niño y El Niño Modoki. *Revista de la Academia Colombiana de Ciencias Exactas, Físicas y Naturales*, 42, 410. https://doi.org/10.18257/raccefyn.705.

Terray, P., Delecluse, P., Labattu, S. and Terray, L. (2003) Sea surface temperature associations with the late Indian summer monsoon. *Climate Dynamics*, 21, 593–618. https://doi.org/10.1007/s00382-003-0354-0.

Timmermann, A., An, S.I., Kug, J.S., Jin, F.F., Cai, W., Capotondi, A., Cobb, K., Lengaigne, M., McPhaden, M.J., Stuecker, M.F., Stein, K., Wittenberg, A.T., Yun, K.S., Bayr, T., Chen, H.C., Chikamoto, Y., Dewitte, B., Dommenget, D., Grothe, P., Guilyardi, E., Ham, Y.G., Hayashi, M., Ineson, S., Kang, D., Kim, S., Kim, W.M., Lee, J.Y., Li, T., Luo, J.J., McGregor, S., Planton, Y., Power, S., Rashid, H., Ren, H.L., Santoso, A., Takahashi, K., Todd, A., Wang, G., Wang, G., Xie, R., Yang, W.H., Yeh, S.W., Yoon, J., Zeller, E. and Zhang, X. (2018) El Niño–Southern Oscillation complexity. *Nature*, 559, 535–545. https://doi.org/10.1038/s41586-018-0252-6.

Torrealba, E. and Amador, J.A. (2010) La corriente en chorro de bajo nivel sobre los Llanos Venezolanos de Sur La corriente en chorro de bajo nivel sobre los Llanos Venezolanos de Sur América. *Revista de Climatología*, 10, 1–20.

Vernekar, A.D., Kirtman, B.P. and Fennessy, M.J. (2003) Low-level jets and their effects on the South American summer climate as simulated by the NCEP Eta model. *Journal of Climate*, 16, 297–311. https://doi.org/10.1175/1520-0442(2003)016<0297:LLJATE>2.0.CO;2.

Viegas, J., Andreoli, R.V., Kayano, M.T., Candido, L.A., de Souza, R. A.F., Hall, D.H., de Souza, A.C., Garcia, S.R., Temoteo, G.G. and Valentin, W.I.D. (2019) Caracterização dos Diferentes Tipos de El Niño e seus Impactos na América do Sul a Partir de Dados Observados e Modelados. *Revista Brasileira de Meteorologia*, 34, 43–67. https://doi.org/10.1590/0102-7786334015.

Wang, H. and Fu, R. (2007) The influence of Amazon rainfall on the Atlantic ITCZ through convectively coupled Kelvin waves. *Journal of Climate*, 20, 1188–1201. https://doi.org/10.1175/JCLI4061.1.

Xie, Z., Duan, A. and Tian, Q. (2017) Weighted composite analysis and its application: an example using ENSO and geopotential height. *Atmospheric Science Letters*, 18, 435–440. https://doi.org/10.1002/asl.786.

Yepes, J., Poveda, G., Mejía, J.F., Moreno, L. and Rueda, C. (2019) Choco-jex: a research experiment focused on the Chocó low-level jet over the far eastern Pacific and western Colombia. *Bulletin of the American Meteorological Society*, 100, 779–796. https://doi.org/10.1175/BAMS-D-18-0045.1.

SUPPORTING INFORMATION

Additional supporting information may be found in the online version of the article at the publisher's website.

How to cite this article: Builes-Jaramillo, A., Yepes, J., & Salas, H. D. (2022). The Orinoco low-level jet during El Niño–Southern Oscillation. *International Journal of Climatology*, 1–15. https://doi.org/10.1002/joc.7681

LISTADO REVISTAS HOMOLOGADAS

No.	NOMBRE	ISSN	CATEGORIA	VIGENCIA	LISTA_SIR
2820	JOURNAL OF AGING AND HEALTH	0898-2643; 1552-6887	A1	Enero 2022 - Diciembre 2022	Index Medicus; PsycINFO; Scimago Journal Rank - SJR; Journal Citation Reports - JCR
2821	JOURNAL OF NEUROSURGICAL ANESTHESIOLOGY	0898-4921; 1537-1921	A1	Enero 2022 - Diciembre 2022	Index Medicus; Scimago Journal Rank - SJR; Journal Citation Reports - JCR
2822	ENTREPRENEURSHIP AND REGIONAL DEVELOPMENT	0898-5626; 1464-5114	A1	Enero 2022 - Diciembre 2022	Scimago Journal Rank - SJR; Journal Citation Reports - JCR
2823	PEDIATRIC PHYSICAL THERAPY	0898-5669; 1538-005X	A1	Enero 2022 - Diciembre 2022	Index Medicus; Scimago Journal Rank - SJR; Journal Citation Reports - JCR
2824	STUDIES IN AMERICAN POLITICAL DEVELOPMENT	0898-588X; 1469-8692	A1	Enero 2022 - Diciembre 2022	Scimago Journal Rank - SJR; Journal Citation Reports - JCR
2825	LINGUISTICS AND EDUCATION	0898-5898; 1873-1864	A1	Enero 2022 - Diciembre 2022	PsycINFO; Arts and Humanities Citation Index (AHCI); Scimago Journal Rank - SJR; Journal Citation Reports - JCR
2826	JOURNAL OF COGNITIVE NEUROSCIENCE	0898-929X; 1530-8898	A1	Enero 2022 - Diciembre 2022	Index Medicus; PsycINFO; Scimago Journal Rank - SJR; Journal Citation Reports - JCR
2827	ACCOUNTABILITY IN RESEARCH ETHICS INTEGRITY AND POLICY	0898-9621; 1545-5815	A1	Enero 2022 - Diciembre 2022	Index Medicus; Scimago Journal Rank - SJR; Journal Citation Reports - JCR
2828	JOURNAL OF MATERIALS IN CIVIL ENGINEERING	0899-1561; 1943-5533	A1	Enero 2022 - Diciembre 2022	Scimago Journal Rank - SJR; Journal Citation Reports - JCR
2829	COMPUTER SCIENCE EDUCATION	0899-3408; 1744-5175	A1	Enero 2022 - Diciembre 2022	Scimago Journal Rank - SJR
2830	NONPROFIT AND VOLUNTARY SECTOR QUARTERLY	0899-7640; 1552-7395	A1	Enero 2022 - Diciembre 2022	Scimago Journal Rank - SJR; Journal Citation Reports - JCR
2831	NEURAL COMPUTATION	0899-7667; 1530-888X	A1	Enero 2022 - Diciembre 2022	Index Medicus; PsycINFO; Scimago Journal Rank - SJR; Journal Citation Reports - JCR
2832	INFECTION CONTROL HOSPITAL EPIDEMIOLOGY	0899-823X; 1559-6834	A1	Enero 2022 - Diciembre 2022	Index Medicus; Scimago Journal Rank - SJR; Journal Citation Reports - JCR
2833	GAMES AND ECONOMIC BEHAVIOR	0899-8256; 1090-2473	A1	Enero 2022 - Diciembre 2022	PsycINFO; Scimago Journal Rank - SJR; Journal Citation Reports - JCR
2834	INTERNATIONAL JOURNAL OF CLIMATOLOGY	0899-8418; 1097-0088	A1	Enero 2022 - Diciembre 2022	Scimago Journal Rank - SJR; Journal Citation Reports - JCR
2835	PEDIATRIC EXERCISE SCIENCE	0899-8493; 1543-2920	A1	Enero 2022 - Diciembre 2022	Index Medicus; Scimago Journal Rank - SJR; Journal Citation Reports - JCR
2836	AIDS EDUCATION AND PREVENTION	0899-9546; 1943-2755	A1	Enero 2022 - Diciembre 2022	Index Medicus; PsycINFO; Scimago Journal Rank - SJR; Journal Citation Reports - JCR
2837	INTERNATIONAL JOURNAL OF ORAL AND MAXILLOFACIAL SURGERY	0901-5027; 1399-0020	A1	Enero 2022 - Diciembre 2022	Index Medicus; Scimago Journal Rank - SJR; Journal Citation Reports - JCR
2838	SCANDINAVIAN JOURNAL OF THE OLD TESTAMENT	0901-8328; 1502-7244	A1	Enero 2022 - Diciembre 2022	Arts and Humanities Citation Index (AHCI); Scimago Journal Rank - SJR
2839	EUROPEAN RESPIRATORY JOURNAL	0903-1936; 1399-3003	A1	Enero 2022 - Diciembre 2022	Index Medicus; Scimago Journal Rank - SJR; Journal Citation Reports - JCR
2840	APMIS	0903-4641	A1	Enero 2022 - Diciembre 2022	Index Medicus; Scimago Journal Rank - SJR; Journal Citation